Primary intracranial extraskeletal myxoid chondrosarcoma in a teenager with unusual frontal location and surgical complications: A case report and literature review

HELU WANG[1], FANG WANG[2] and HONGTAO ZHANG[3]

[1]School of Clinical Medicine, Shandong Second Medical University, Weifang, Shandong 261000, P.R. China;
[2]Department of Pathology, The Affiliated Yantai Yuhuangding Hospital of Qingdao University, Yantai, Shandong 264000, P.R. China;
[3]Department of Neurosurgery, Yantai Yuhuangding Hospital, Yantai, Shandong 264000, P.R. China

Received July 29, 2025; Accepted October 27, 2025

DOI: 10.3892/ol.2025.15437

Abstract. Primary intracranial extraskeletal myxoid chondrosarcoma (EMC) is rare and diagnostically challenging, with only sporadic pediatric and adolescent cases reported. The current study describes the case of a 17-year-old male presenting with an acute headache, nausea and emesis. Neuroimaging revealed a 7.2x5.2-cm hemorrhagic mass in the right frontal lobe with involvement of the anterior skull base. A gross total resection was achieved. Histopathology confirmed EMC with high-grade features, including loss of integrase interactor 1 (INI1) expression and a Ki-67 labeling index of 80%. The postoperative course was complicated by bacterial meningitis, which resolved with antibiotics. Adjuvant radiotherapy was delivered to the tumor bed and involved the dura at 66 Gy in 33 fractions without major toxicity. At the 3-month follow-up, there was no evidence of recurrence. This presentation, namely frontal-lobe localization in an adolescent and an aggressive immunophenotype with INI1 loss, is uncommon for intracranial EMC, which is more frequently described in middle-aged patients and posterior fossa sites. Molecular subtyping, which can inform targeted therapy selection, was not performed due to financial constraints. The diagnosis relied on multimodal integration of imaging, histology and immunohistochemistry; key mimics were disfavored by negative staining for glial fibrillary acidic protein, epithelial membrane antigen, desmin and S-100 protein. Given the pathological risk profile and the anticipated limited benefit of chemotherapy, systemic therapy was not pursued. The patient's long-term prognosis remains uncertain, and imaging surveillance is planned at 3- to 6-month intervals for 2 years and annually thereafter. This case highlights the importance of considering EMC in the differential diagnosis of young patients presenting with aggressive, hemorrhagic intracranial masses, particularly those with INI1 loss, and underscores the need for multimodal diagnostic approaches in such rare entities.

Correspondence to: Professor Hongtao Zhang, Department of Neurosurgery, Yantai Yuhuangding Hospital, 20 Yudong Road, Zhifu, Yantai, Shandong 264000, P.R. China
E-mail: doctorzht@163.com

Abbreviations: EMC, extraskeletal myxoid chondrosarcoma; MRI, magnetic resonance imaging; RT, radiotherapy

Key words: extraskeletal myxoid chondrosarcoma, adolescent brain tumor, frontal lobe tumor, high-grade sarcoma, immunohistochemistry

Introduction

Extraskeletal myxoid chondrosarcoma (EMC) is a rare, clinicopathologically distinct soft-tissue sarcoma and a subtype of chondrosarcoma, and it represents a malignant mesenchymal neoplasm of uncertain differentiation and exceptional rarity, accounting for <3% of all soft-tissue sarcomas, with an annual incidence of ~1 per million individuals. EMC is characterized histologically by bland-appearing spindle to stellate cells arranged in cords, reticular or lace-like patterns within abundant myxoid stroma and typically, a lack of overt hyaline cartilage differentiation (1). EMC most commonly arises in the deep soft tissues of the proximal limbs in middle-aged to older adults, predominantly affecting middle-aged adults (median age, 50 years) and showing a male-to-female ratio of ~2:1, with a predilection for the thigh and popliteal fossa, and less frequent involvement of the trunk (2). Despite its deceptively bland cytology, EMC has been associated with substantial risks of local recurrence and distant metastasis, most often to the lungs and soft tissues. Recurrent chromosomal rearrangements involving the nuclear receptor subfamily 4 group A member 3 (*NR4A3*) gene on chromosome 9q22 have emerged as highly characteristic and diagnostically informative hallmarks. The classic translocation is t(9;22)(q22;q12), which fuses Ewing sarcoma breakpoint region 1 (*EWSR1*) with nuclear receptor subfamily 4 group A member 3 (*NR4A3*). Other variant partners include TATA-box binding protein associated factor 15 (*TAF15*), rearranged through t(9;17)(q22;q11), and less commonly, transcription factor 12 (TCF12), involved in t(9;15)(q22;q21) (3,4). By contrast, primary intracranial EMC is exceedingly rare and has been reported to arise

from the meninges or, less commonly, the brain parenchyma; its clinical and radiological features frequently overlap with meningioma, glioma and other sarcomas, complicating the formation of an accurate diagnosis (5). In the absence of large series and standardized treatment protocols, evaluation relies on integrated assessment combining imaging, histopathology and, where available, molecular genetics. The present study reports a case of adolescent intracranial EMC with high-grade features and outlines the diagnostic pitfalls and management considerations pertinent to this uncommon entity.

Case report

In April 2025, a 17-year-old male patient presented to the Department of Neurosurgery at Yantai Yuhuangding Hospital (Yantai, China) with a 1-week history of a progressive headache that had acutely worsened over the preceding 24 h, accompanied by nausea and emesis. A neurological examination showed impaired orientation, calculation and memory. The pupils measured 3 mm bilaterally, limb strength was Medical Research Council grade 5- and no pathological reflexes were elicited (6). Non-contrast head computed tomography (CT) scans taken in an external hospital revealed a right frontal space-occupying lesion, with intracranial neoplasm and stroke considered in the initial differential.

On hospital day 2, contrast-enhanced 3T magnetic resonance imaging (MRI) demonstrated a 7.2x5.2-cm right frontal mass with intralesional hemorrhage and mass effect displacing the anterior and middle cerebral arteries (Fig. 1). CT angiography additionally suggested anterior skull-base involvement with adjacent dural contact (Fig. 2). A working diagnosis of a tumor-related stroke was considered; oligodendroglioma and meningioma were included in the differential.

On hospital day 5, after exclusion of surgical contraindications, the patient underwent a craniotomy for tumor resection. Intraoperatively, a solid, firm, hypervascular mass without a discrete capsule was identified with invasion of the anterior skull-base dura. Fluorescein sodium aided delineation of the tumor-brain interface, and a gross total resection was achieved. The cut surface was soft and gelatinous. Dural defects were repaired with artificial dura. Postoperatively, the patient was transferred to the intensive care unit for ventilatory support.

At 24 h post-surgery, the patient was somnolent with a Glasgow Coma Scale score of E3V5M6 and proximal limb strength of 5- (6,7). Follow-up CT demonstrated a hematoma with progressive fluid accumulation within the resection cavity when compared with immediate postoperative imaging. By postoperative day 3, after discontinuation of therapeutic hypothermia, the patient's temperature peaked at 37.5˚C and the clinical status stabilized, permitting transfer to the general ward.

On postoperative day 5, a high-grade fever and incisional discharge prompted a lumbar puncture, which showed elevated opening pressure and marked cerebrospinal-fluid pleocytosis. Culture of the fluid grew methicillin-resistant *Staphylococcus aureus*, confirming postoperative bacterial meningitis. The patient received intravenous meropenem (1 g every 8 h) and vancomycin (1 g every 12 h); defervescence and wound resolution were achieved after 6 days.

On postoperative day 16, histopathological analysis established a diagnosis of EMC. Tissue samples were fixed in 4% Paraformaldehyde Fix Solution (cat. no. P0099-500 ml; Beyotime Biotechnology) at room temperature for 24 h, followed by routine dehydration and embedding in paraffin. Sections were cut at a thickness of 3 μm and mounted on slides. To minimize non-specific background, sections were blocked with 3% bovine serum albumin in PBS for 1 h at room temperature. The Roche BenchMark automated staining platform was used according to the manufacturer's instructions, with the following ready-to-use primary antibodies, incubated at room temperature for 32 min: p53 (cat. no. 61209507; Beijing Zhongshan Jinqiao Biotechnology Co., Ltd.), vimentin (cat. no. ZM-0260; Beijing Zhongshan Jinqiao Biotechnology Co., Ltd.), Ki-67 (Gene Tech Co., Ltd.; cat. no. GT209407), CK(Pan) (GeneTech Co., Ltd.; cat. no. GM351507), INI1 (Beijing Zhongshan Jinqiao Biotechnology Co., Ltd.; cat. no. ZA-0696), S100 (Beijing Zhongshan Jinqiao Biotechnology Co., Ltd.; cat. no. ZA-0225), Desmin (GeneTech Co., Ltd.; cat. no. GT225207), EMA (Thermo Fisher Scientific, Inc.; cat. no. 24 h-0095), GFAP (cat. no. ZM-0118; Beijing Zhongshan Jinqiao Biotechnology Co., Ltd.), synaptophysin (cat. no. ZM-0246; Beijing Zhongshan Jinqiao Biotechnology Co., Ltd.), CD34 (GeneTech Co., Ltd.; cat. no. GM716507), IDH1 (Beijing Zhongshan Jinqiao Biotechnology Co., Ltd.; cat. no. ZM-0447), SOX10 (cat. no. ZA-0624; Beijing Zhongshan Jinqiao Biotechnology Co., Ltd.), STAT6 (cat. no. ZA-0647; Beijing Zhongshan Jinqiao Biotechnology Co., Ltd.), NKX2.2 (cat. no. ZA-0655; Beijing Zhongshan Jinqiao Biotechnology Co., Ltd.) and SMA (cat. no. Kit-0006/MAB-0890; Abcam). Immunohistochemical analysis showed the following results: S-100(-), integrase interactor 1 (INI1)(-), cytokeratin (CK)(-), smooth muscle actin (SMA)(-), desmin(-), CD34(-), STAT6(-), homeobox protein Nkx-2.2 (NKX2.2)(-), transcription factor SOX-10 (SOX10)(-), synaptophysin(-), epithelial membrane antigen (EMA)(-), glial fibrillary acidic protein (GFAP)(-), diffuse vimentin(+), p53(+, 60%), isocitrate dehydrogenase 1 (IDH-1)(-) and a Ki-67 labeling index of 80% (Figs. 3-5). NR4A3 fluorescence *in situ* hybridization (FISH) was recommended to confirm the molecular subtype, but was declined due to financial constraints and concerns about invasive testing.

After discontinuation of intensive antimicrobial therapy, the patient remained afebrile. Following a 23-day hospitalization period, the patient was discharged with baseline neurological function restored. Discharge medications included 30 mg oral idebenone three times daily and 0.2 g oral citicoline sodium three times daily; neurosurgical follow-up was scheduled for surveillance.

Approximately 1 month postoperatively, the patient was readmitted for adjuvant radiotherapy (RT). Baseline hematological parameters were within reference ranges: Red blood cells, 4.71×10^{12}/l (normal range, 4.0-5.5x10^{12}/l); hemoglobin, 142 g/l (normal range, 130-175 g/l); platelets, 285×10^{9}/l (normal range, 125-350x10^{9}/l); and leukocytes, 8.36×10^{9}/l (normal range, 4.0-10.0x10^{9}/l).

Simulation CT (3-mm slice thickness) was acquired with the patient in a supine position and immobilized in a thermoplastic mask. The tumor bed and contrast-enhancing region were contoured as the gross tumor volume with a 3-mm margin to generate the planning gross tumor volume (59.40 Gy in 33 fractions). Preoperative edema and enhancing dura defined the clinical target volume; a further 3-mm margin

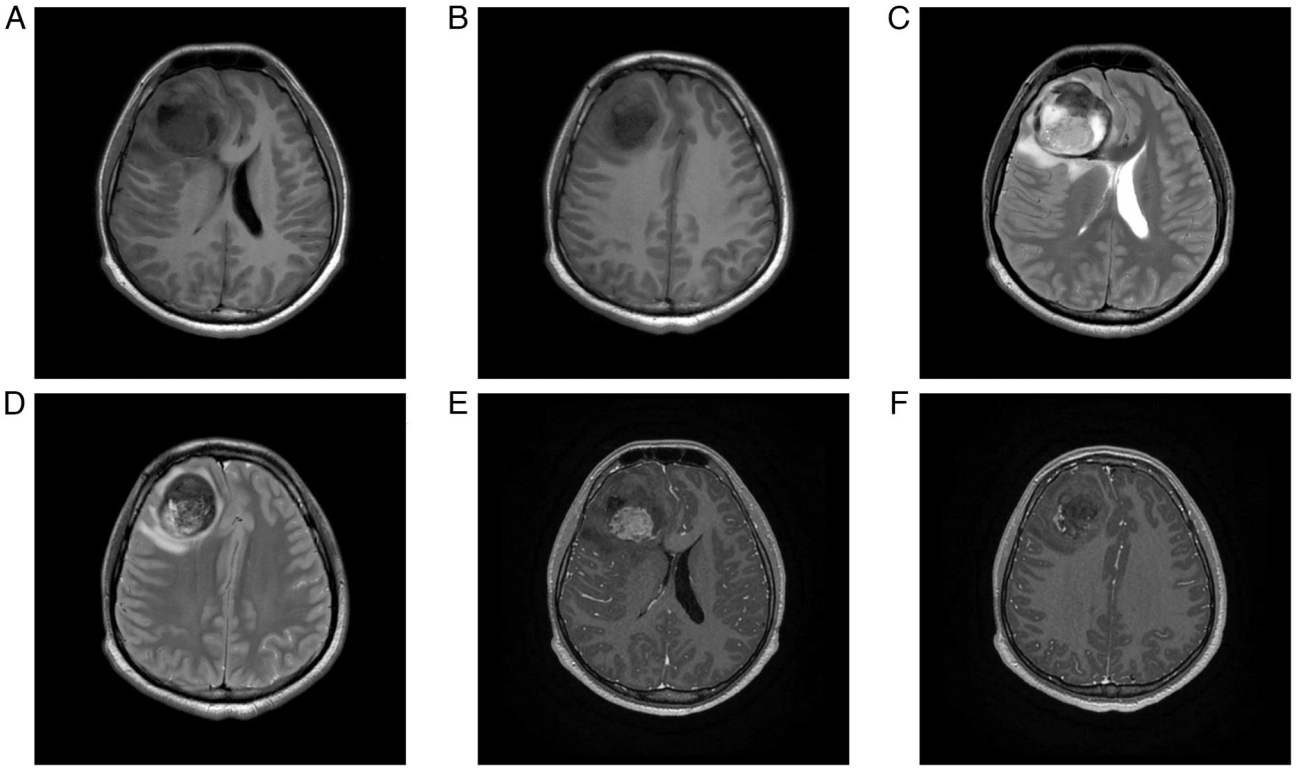

Figure 1. Preoperative magnetic resonance imaging. (A) Axial T1WI demonstrating a quasi-round, slightly hypointense lesion in the right frontal lobe with ill-defined margins. (B) Axial T1WI revealing heterogeneous intralesional signal intensity. (C) Axial T2WI showing a slightly hyperintense lesion obscuring the normal gray-white matter differentiation. (D) Axial T2WI illustrating mild lobulation at the lesion margin. (E) Axial contrast-enhanced T1WI demonstrating irregular annular and nodular enhancement. (F) Coronal contrast-enhanced T1WI revealing a central non-enhancing necrotic core with adjacent linear dural enhancement. WI, weighted imaging.

Figure 2. Preoperative CT. (A) Axial non-contrast CT showing a mixed-density mass in the right frontal lobe (~5.0x5.2 cm). (B) The lesion has well-defined borders with peripheral annular hyperdensity and internal punctate calcifications. (C) Extensive surrounding parenchymal hypodensity, consistent with vasogenic edema, resulting in a significant leftward midline shift. CT, computed tomography.

produced the planning target volume (PTV) (66 Gy in 33 fractions). Treatment-planning verification confirmed ≥95% isodose coverage of the PTV with organ-at-risk doses within institutional constraints.

Hematological indices were monitored throughout RT and showed a mild downward trend consistent with non-actionable myelosuppression (week 7: hemoglobin, 140 g/l; platelets, $238x10^9$/l; and leukocytes, $4.83x10^9$/l). No laboratory threshold for intervention was reached.

During the course of radiotherapy, adjunctive osmotherapy with intravenous 20% mannitol (125 ml every 8 h) was administered to manage perilesional edema. The patient's Eastern Cooperative Oncology Group performance status remained at 1 (8), and no radiation-induced dermatitis or neurological toxicity was observed.

Post-RT MRI demonstrated substantial resolution of the postoperative hematoma and associated fluid collections (Fig. 6). Given the high-risk pathological features (INI1 loss and Ki-67 at 80%) and the limited responsiveness of EMC to conventional chemotherapy reported in the literature, a multidisciplinary team concluded that adjuvant chemotherapy would provide no clear clinical benefit; systemic therapy was

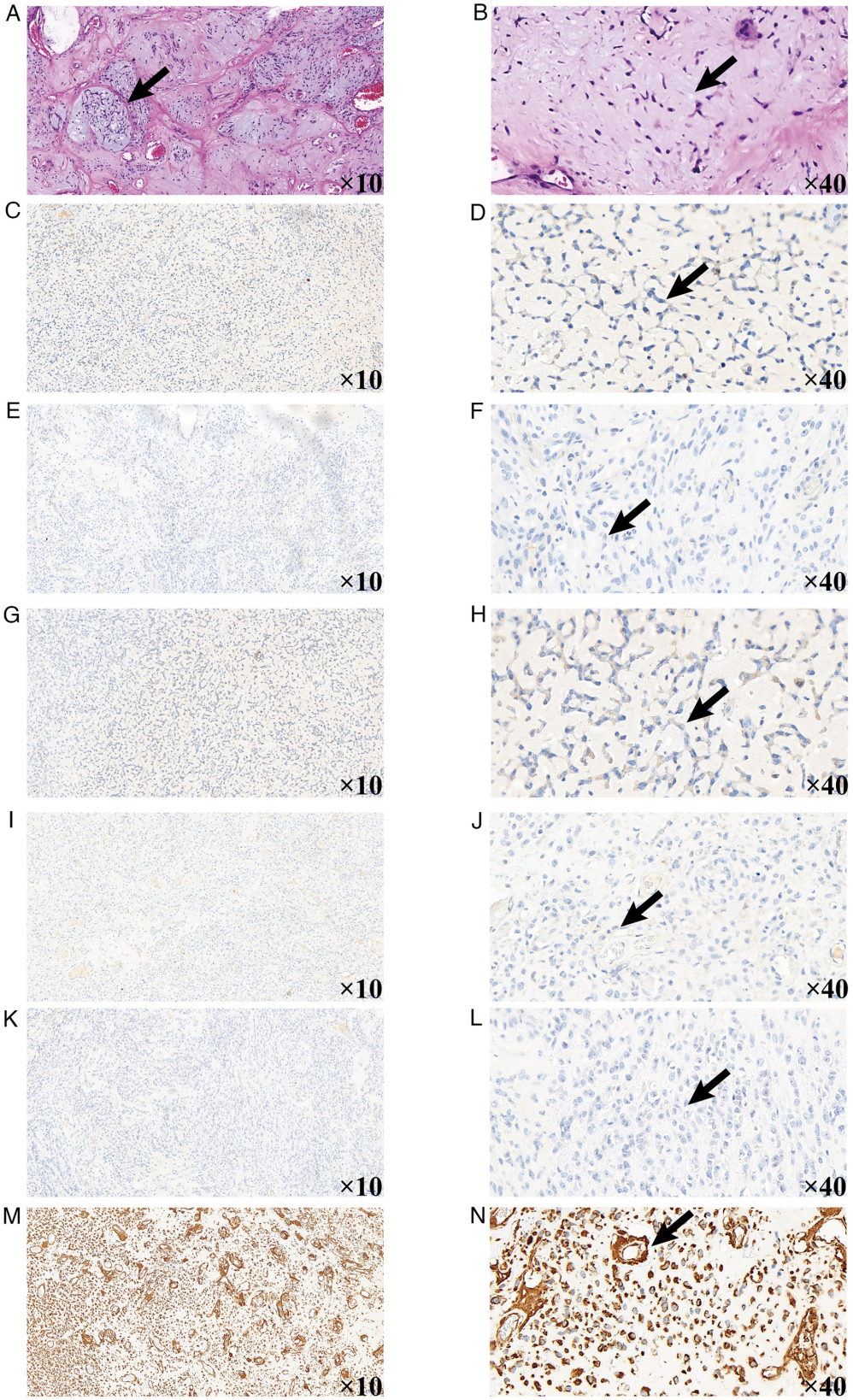

Figure 3. Histopathology and immunohistochemistry findings. Hematoxylin-eosin staining images at (A) x10 and (B) x40 magnification demonstrating a predominantly nodular growth pattern with variable cellular density. Hypocellular regions contain abundant myxoid stroma with tumor cells arranged in cord-like and reticular patterns. Hypercellular regions show diffusely distributed cells, predominantly oval to short spindle-shaped in morphology, with pronounced pleomorphism and significant atypia. Mitotic figures are easily observed, with prominent small red nucleoli. The cytoplasm is scant, with some cells displaying vacuolation. Immunohistochemistry for cytokeratin showing negative staining at (C) x10 and (D) x40 magnification. Immunohistochemistry for S-100 showing negative staining at (E) x10 and (F) x40 magnification. Immunohistochemistry for desmin showing negative staining at (G) x10 and (H) x40 magnification. Immunohistochemistry for epithelial membrane antigen showing negative staining at (I) x10 and (J) x40 magnification. Immunohistochemistry for glial fibrillary acidic protein showing negative staining at (K) x10 and (L) x40 magnification. Immunohistochemistry for vimentin showing positive staining at (M) x10 and (N) x40 magnification. Arrows indicate representative tumor areas of staining. All sections were obtained from the resected intracranial mass, and are formalin-fixed paraffin-embedded tissues, with hematoxylin counterstain. Scale bar, 100 μm.

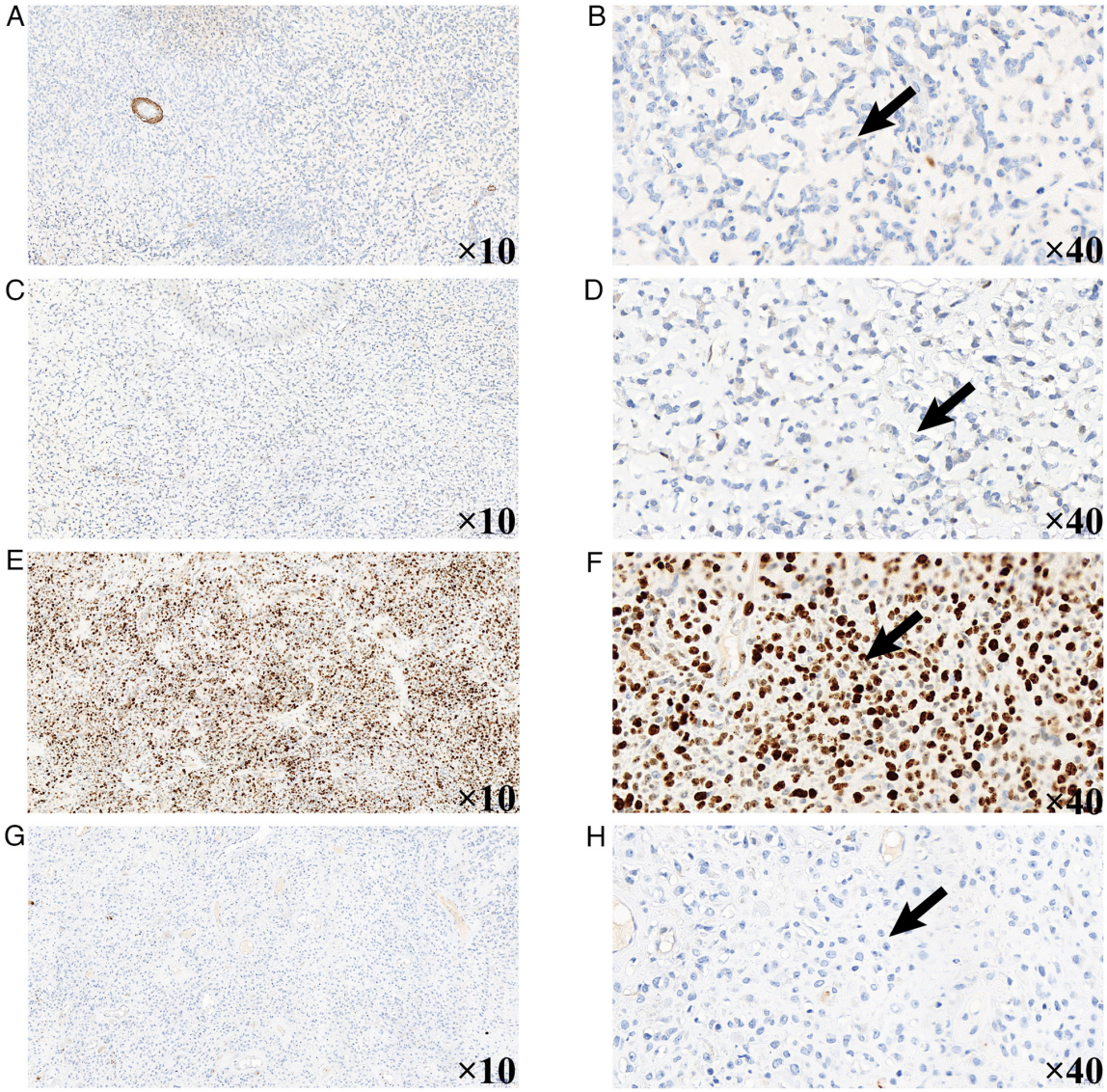

Figure 4. Histopathology and immunohistochemistry findings. Immunohistochemistry images for smooth muscle actin showing negative staining at (A) x10 and (B) x40 magnification. immunohistochemistry for INI-1 showing complete loss of nuclear expression (negative) at (C) x10 and (D) x40 magnification. Immunohistochemistry for Ki-67 demonstrating a markedly elevated proliferation index, reaching ~80% in the most active regions, at (E) x10 and x40 (F) magnification. Immunohistochemistry for synaptophysin showing negative staining at (G) x10 and (H) x40 magnification. Arrows indicate representative tumor areas of staining. All sections were obtained from the resected intracranial mass, and are formalin-fixed paraffin-embedded tissue, with hematoxylin counterstain. Scale bar, 100 μm.

therefore not pursued, and the patient was discharged. The patient's long-term prognosis remains uncertain, and imaging surveillance is planned at 3- to 6-month intervals for 2 years and annually thereafter.

Discussion

EMC is a rare soft-tissue sarcoma, accounting for 2.5-3% of all soft-tissue sarcomas. EMC is classified by the World Health Organization as a 'mesenchymal tumor of uncertain differentiation' (9). Pathologically, EMC exhibits a multinodular architecture with a mucin-rich matrix and chondroid cells showing malignant cytological features (10). Although initially regarded as a low-grade neoplasm, subsequent studies have shown a notable propensity for local recurrence and distant metastasis (11,12), particularly to the lungs (13). Intracranial EMC is hypothesized to arise from embryonic remnants within cranial bones or from pluripotent mesenchymal cells in the dura mater (14). EMC most often affects middle-aged men and typically presents as a slowly enlarging, painless, deep-seated mass in the proximal limbs (9). By contrast, intracranial lesions usually have an insidious onset with non-specific symptoms, frequently delaying the diagnosis.

The present study reports a rare case of intracranial EMC in a 17-year-old male patient; to the best of our knowledge, only 16 comparable cases have been reported worldwide (Table I). The present case adds to the spectrum of primary intracranial EMC, a review of which is summarized in Table I (5,14-28). The current patient presented with an acute headache, in contrast to the classically indolent course of EMC. Imaging disclosed a large right frontal mass (7.2x5.2 cm) with intralesional hemorrhage and invasion of the anterior cranial-fossa dura.

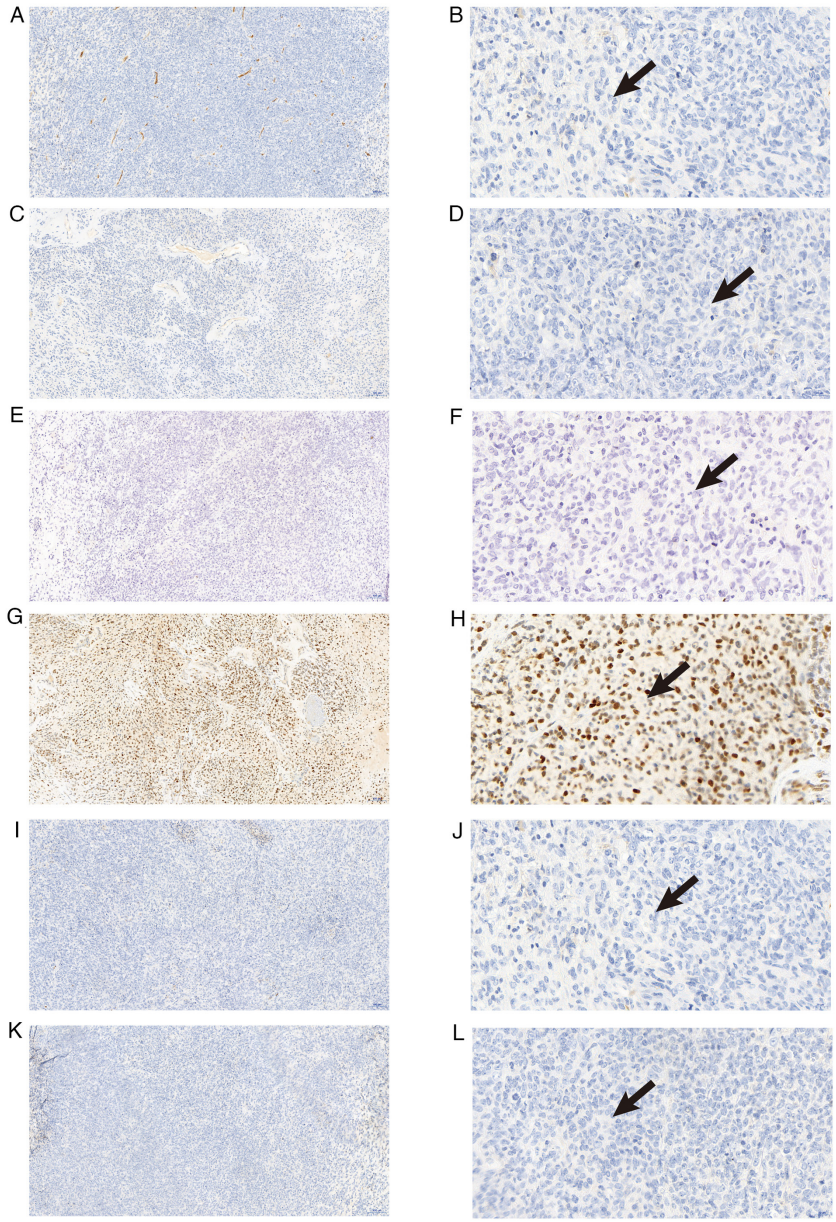

Figure 5. Histopathology and immunohistochemistry findings. Immunohistochemistry images for CD34 showing negative staining at (A) x10 and (B) x40 magnification. Immunohistochemistry images for IDH-1 showing negative staining at (C) x10 and (D) x40 magnification. Immunohistochemistry images for NKX2.2 showing negative staining at (E) x10 and (F) x40 magnification. Immunohistochemistry images for p53 showing positive nuclear expression (+, 60%) at (G) x10 and (H) x40 magnification. Immunohistochemistry images for SOX-10 showing negative staining at (I) x10 and (J) x40 magnification. Immunohistochemistry images for STAT6 showing negative staining at (K) x10 and (L) x40 magnification. Arrows indicate representative tumor areas of staining. All sections were obtained from the resected intracranial mass and are formalin-fixed paraffin-embedded tissues, with hematoxylin counterstain. Scale bar, 100 μm.

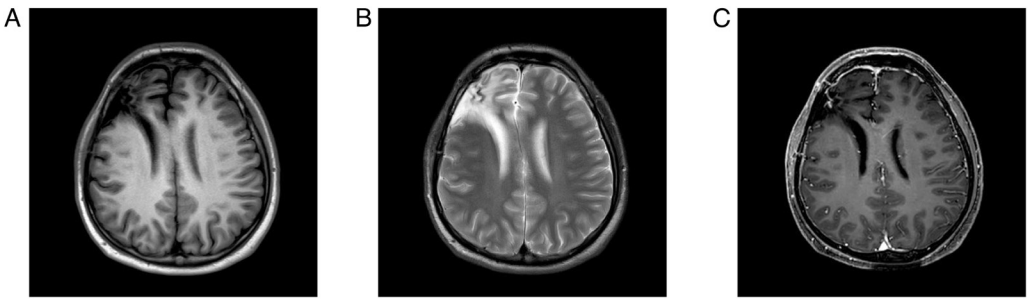

Figure 6. Follow-up magnetic resonance imaging at 3 months postoperatively. (A) T1-weighted image showing an irregularly shaped surgical cavity in the right frontal region with hypointense signal; discontinuity of the right frontal bone is noted, compatible with a postoperative change/bone defect. (B) T2-weighted image showing a hyperintense signal within the surgical cavity and patchy edema in the adjacent right frontal lobe parenchyma. (C) Contrast-enhanced T1-weighted image showing thickening and enhancement of the cavity margin and adjacent dura mater, with focal nodular enhancement.

Table I. Reported cases of primary intracranial extraskeletal myxoid chondrosarcoma.

First author/s, year	Sex	Age, years	Clinical symptoms	Size, cm	Locations of tumor	Treatment	Recurrence	Metastasis	(Refs.)
Scott *et al*, 1976	M	39	Headache, nausea and vomiting	NA	4th ventricle	PR	N	N	(15)
Smith and Davidson, 1981	M	12	Headache, nausea, vomiting and difficulty ambulating	3.5x1.0x0.5	Left cerebellum	GTR	N	N	(16)
Salcman *et al*, 1992	F	28	Headache, slow speech and right limb weakness	7.0x5.0x4.0	Left parafalcine region	GTR	Y	N	(17)
Sato *et al*, 1993	F	43	Blurred vision and gait disturbance	NA	Pineal region	PR, RT (60 Gy), chemotherapy	Y	Y	(18)
Chaskis *et al*, 2002	F	17	Headache and status epilepticus	NA	Right frontal-parietal lobe	GTR	Y	N	(14)
González-Lois *et al*, 2002	M	69	Headache, dizziness and behavior change	NA	Right frontal lobe	GTR	N	N	(19)
Im *et al*, 2003	M	43	Headache, nausea and vomit	2.0	Left parietal lobe	GTR, RT (59.4 Gy)	N	N	(20)
Cummings *et al*, 2004	M	63	Hearing loss and gait disturbance	2.4x1.8x2.4	Right jugular foramen, right Cerebellopontine Angle (CPA)	GTR	NA	NA	(21)
Sorimachi *et al*, 2008	F	37	Headache, nausea, vomit and upward gaze palsy	NA	Pineal region	GTR, RT (59.4 Gy)	N	N	(22)
O'Brien *et al*, 2008	F	26	Headache, nausea and seizure	2.5	Left CPA	STR proton therapy	N	N	(23)
Arpino *et al*, 2011	F	54	Headache and left ophthalmoplegia	NA	Sellar and parasellar area	GTR	NA	NA	(24)
Dulou *et al*, 2012	F	70	Behavior change and difficulty in walking	NA	Left frontal lobe	GTR, preoperative RT (60 Gy)	Y	N	(25)
Park *et al*, 2012	F	21	Headache, right limb weakness, bilateral hearing loss and bilateral vision loss	3.2x6.3x4.9	Left lateral ventricle	GTR, RT (60.8 Gy)	NA	NA	(26)
Qin *et al*, 2017	F	41	Headache and vomiting	3.0x3.0x3.0	Left cerebellum	GTR, two stage RT (56 Gy/50 Gy), chemo	N	N	(27)
Akakin *et al*, 2018	F	75	Right limb weakness	NA	Left parafalcine region	GTR	Y	N	(28)
Zhu *et al*, 2022	M	52	Headache, dizzy and nausea	3.4x3.0	Left cavernous sinus	GTR, RT (45 Gy)	N	N	(5)
Present case	M	17	Headache, nausea and vomiting	7.2x5.2	Right frontal lobe	GTR, RT (59.4 Gy)	N	N	

NA, not available; PR, partial resection; STR, subtotal resection; GTR, gross total resection; N, no; Y, yes; CPA, cerebellopontine angle; RT, radiotherapy.

Table II. Immunohistochemical features of intracranial myxoid chondrosarcomas in reported cases.

First author, year	GFAP	Cytokeratin	EMA	S-100	Vimentin	NSE	Synapto-physin	Chromo-granin A	(Refs.)
Smith and Davidson, 1981	(-)								(16)
Salcman *et al*, 1992	(-)	(-)	(-)	(-)	(++)				(17)
Sato *et al*, 1993	(-)			(++)	(++)				(18)
González-Lois *et al*, 2002	(+)	(-)	(-)	(+), focal	(+)	(-)			(19)
Im *et al*, 2003	(-)	(-)	(-)	(+), weak	(+)				(20)
Sorimachi *et al*, 2008	(-)	(-)	(-)	(-)	(+)	(-)	(-)	(-)	(22)
O'Brien *et a*l, 2008	(-)	(-)	(-)	(-)	(-)	(-)	(-)	(-)	(23)
Park *et al*, 2012	(-)	(+), focal strong	(+)	(+)					(26)
Dulou *et al*, 2012	(+)	(+), strong	(+), weak						(25)
Qin *et al*, 2017	(-)	(-)	(-)	(+)					(27)
Akakin *et al*, 2018	(-)	(-)	(+)	(+)	(+)	ND	(-)	(-)	(28)
Zhu *et al*, 2022	(-)	(-)	(-)	(+)	(+)	ND	ND	ND	(5)
Present case	(-)	(-)	(-)	(-)	(+)	ND	(-)	ND	

Studies with fewer than two tested markers were excluded from the table. GFAP, glial fibrillary acidic protein; EMA, epithelial membrane antigen; NSE, neuron-specific enolase.

Notably, the supratentorial location challenges the conventional expectation that intracranial EMCs predominantly arise in the posterior cranial fossa; fewer than 5 supratentorial cases have been documented (17,28). Postoperative histopathology confirmed EMC with loss of INI1 expression and a high Ki-67 labeling index (80%), indicating an aggressive phenotype. The distinctiveness of this case lies in its adolescent onset (typical onset, 50-60 years), right frontal location and high proliferative activity with INI1 loss. The postoperative course was further complicated by bacterial meningitis, adding to the management complexity.

The present case underscores the pronounced clinical and pathological heterogeneity of EMC. An accurate diagnosis requires an integrated, multimodal assessment. Immunohistochemically, the tumor showed diffuse vimentin positivity, consistent with mesenchymal differentiation, and was negative for S-100, aligning with the frequently low rate of S-100 expression reported in intracranial EMCs (28,29) (Table II). The immunohistochemical profile of the present case aligns with reported intracranial EMCs, with a detailed comparison provided in Table II (5,16-20,22,23,25-28).

Histopathological evaluation of hematoxylin and eosin (H&E)-stained sections revealed a hypercellular neoplasm with a multinodular architecture within an abundant myxoid stroma. Tumor cells were predominantly eosinophilic, ranging from epithelioid to plump spindle forms, arranged in cords, nests and reticular patterns. There was marked nuclear atypia, elevated mitotic activity and foci of hemorrhagic change. A panel of negative immunomarkers supported systematic exclusion of mimics: GFAP and SOX10 negativity argued against gliomas and schwannomas (30); CK and EMA negativity argued against epithelial tumors and meningiomas (31); synaptophysin, desmin and SMA negativity argued against neuroendocrine and myogenic neoplasms (32); and the absence of CD34 and STAT6 expression did not support a pericytic/solitary fibrous tumor lineage (33). Furthermore, while CD99 is a valuable marker in the differential diagnosis of small round cell tumors, particularly for excluding Ewing sarcoma, it was not performed in the present retrospective case as the comprehensive diagnostic workup was already achieved through the extensive immunohistochemical panel and characteristic morphological features. However, based on its established role in differential diagnosis, its inclusion is recommended in a routine panel. The hemorrhagic transformation may reflect aberrant vascular proliferation, concordant with the high Ki-67 index (up to 80%) and strong p53 immunoreactivity (>60%), collectively suggesting activated angiogenesis-related pathways.

Loss of INI1 expression is infrequently observed in conventional intracranial EMCs (reported in <10% of cases) but has been described in high-grade morphological variants with pronounced atypia and brisk mitotic activity (34). The combination of characteristic H&E features, multinodular myxoid stroma with corded growth and the specific immunoprofile is strongly supportive of EMC. Diffuse vimentin positivity with absent synaptophysin/EMA expression effectively excludes malignant rhabdoid tumors, while CK negativity argues against chordoma. In addition, negative NKX2.2 and IDH-1 staining disfavors Ewing's sarcoma and IDH-mutant gliomas, respectively (35).

The immunoprofile in the present case, namely strong vimentin positivity, S-100 negativity, synaptophysin negativity

Table III. MRI features of primary intracranial extraskeletal myxoid chondrosarcoma case.

First author, year	T1WI	T2WI	Enhanced MRI	(Refs.)
Scott *et al*, 1976	NA	NA	NA	(15)
Smith and Davidson, 1981	NA	NA	NA	(16)
Salcman *et al*, 1992	Well-defined, hyperintensity	Homogeneous hyperintensity	NA	(17)
Sato *et al*, 1993	NA	NA	NA	(18)
Chaskis *et al*, 2002	Hypointensity	NA	Heterogeneous enhancement	(14)
González-Lois *et al*, 2002	NA	NA	Significantly homogeneous enhancement	(19)
Im *et al*, 2003	Unclear-defined, hypointensity	Hyperintensity	Homogeneously well enhanced	(20)
Cummings *et al*, 2004	NA	NA	Heterogeneous enhancement	(21)
Sorimachi *et al*, 2008	Mixed signal intensity, hyperintensity (hemorrhage)	NA	Heterogeneous enhancement	(22)
O'Brien *et al*, 2008	Hypointensity	Hyperintensity	NA	(23)
Arpino *et al*, 2011	Hypointensity	Hyperintensity	Heterogeneously peripheral enhancement	(24)
Dulou *et al*, 2012	NA	Hyperintensity, peritumor edema	Heterogeneously ring-like enhancement	(25)
Park *et al*, 2012	Homogeneous iso-intensity	Heterogeneous hyperintensity, Peritumor edema	Heterogeneously lobulated enhancement	(26)
Qin *et al*, 2017	NA	NA	NA	(27)
Akakin *et al*, 2018	NA	Heterogeneous hyperintensity	Heterogeneously rim-like enhancement, DWI showed intratumor calcification	(28)
Zhu *et al*, 2022	Homogeneous hypointensity	Heterogeneous hyperintensity	Heterogeneously well enhanced	(5)
Present case	Hypointensity	Hyperintensity	Heterogeneously well enhanced	

MRI, magnetic resonance image; T1WI, T1-weighted imaging; T2WI, T2-weighted imaging; DWI, diffused-weighted imaging; NA, not available.

and the absence of lineage-defining markers, closely mirrors reported intracranial EMCs, including those associated with the TAF15-NR4A3 fusion subtype; in the absence of molecular confirmation, however, this remains inferential. This fusion subtype accounts for ~20% of EMCs and has been linked to aggressive clinical behavior and resistance to pazopanib (36). Molecular confirmation remains rare in the literature, with definitive subtyping reported in only 1 of 16 documented intracranial cases (5). Thus, while the diagnosis is well supported by histomorphology and immunohistochemistry, definitive classification would require genetic confirmation, which was not performed in the present case (5).

A definitive diagnosis typically requires molecular detection of NR4A3 rearrangements, most commonly confirmation of the EWSR1-NR4A3 fusion (37). The patient's refusal to undergo NR4A3 testing imposed two critical limitations: First, the TAF15-NR4A3 subtype, which confers relative resistance to pazopanib, could not be distinguished from the EWSR1-NR4A3 subtype, precluding accurate molecular subtyping; and second, prognostication may be less reliable, as patients with TAF15 fusions have significantly lower 5-year survival rates than those with EWSR1 fusions.

Given the high-risk pathological features, management raised three major challenges. First, postoperative bacterial meningitis, reflected by a cerebrospinal-fluid white-cell count of 836×10^6/l, may necessitate delaying RT, thereby increasing the risk of recurrence. Second, invasion of the skull-base dura complicates margin assessment and favors the judicious use of neuronavigation. Third, in this high-risk context, systemic therapies such as temozolomide or pazopanib merit consideration;

temozolomide penetrates the blood-brain barrier effectively, whereas pazopanib may be more suitable for patients lacking the TAF15 fusion. At the 3-month postoperative follow-up, no recurrence was detected in the present case. Nonetheless, vigilant long-term surveillance is warranted, as distant metastases often emerge years after surgery. Proton-beam therapy may offer dosimetric advantages over conventional RT, but the optimal strategy requires further evaluation (37).

Imaging findings are pivotal for differential diagnosis and require synthesis across modalities. CT typically shows a well-circumscribed hypodense mass, with calcification in ~12.5% of cases (5). Contrast-enhanced CT often demonstrates mild or absent enhancement (2). MRI provides greater diagnostic resolution: Lesions are commonly iso- to hypointense on T1-weighted sequences, with hemorrhagic foci appearing hyperintense (38). On T2-weighted imaging, they are frequently markedly hyperintense with hypointense fibrous septa, often producing a multiloculated cystic appearance (2,39). Post-contrast enhancement is typically septal, ring-like or lobulated; ~10% of cases show minimal or no enhancement (38). The MRI characteristics in the present case align closely with these descriptors (Table III). The imaging findings in the present case are consistent with the spectrum of MRI features summarized in Table III (5,14-28).

Key differential diagnoses of EMC include chondroid meningioma, which often exhibits calcification and a characteristic dural-tail sign (1), ependymoma, which commonly arises in the fourth ventricle and may disseminate along cerebrospinal-fluid pathways (38), cavernous hemangioma, which shows a 'popcorn-like' mixed T2 signal with a surrounding hemosiderin rim, and metastatic tumors, which are frequently multiple and typically associated with substantial vasogenic edema (5).

For clinical practice, heightened vigilance is warranted when encountering intracranial mucin-rich tumors with hemorrhage and skull-base invasion in adolescents. A routine immunohistochemical panel should include vimentin, S-100, CD99 and INI1, with strong consideration of NR4A3 assessment. Molecular confirmation is recommended using FISH or RNA sequencing.

Therapeutically, meticulous control of surgical boundaries at the skull base and timely initiation of RT, at a recommended dose of 50-54 Gy, are crucial. Systemic options may include temozolomide or pazopanib. For patients with a relevant family history, genetic screening should be considered.

The present study has several limitations, including the absence of NR4A3 fusion testing, a short postoperative follow-up of only 3 months and the lack of mechanistic validation. Given that EMC can metastasize years after surgery, long-term standardized follow-up is essential. Future work should prioritize establishing a dedicated registry for adolescent EMCs and investigating age-specific mechanisms, including functional interrogation of the LSM14A-NR4A3 fusion, the consequences of INI1 loss and strategies for combination immunotherapy.

Acknowledgements

Not applicable.

Funding

No funding was received.

Availability of data and materials

The data generated in the present study may be requested from the corresponding author.

Authors' contributions

HW designed and conducted the study, collected the case report data, and analyzed and interpreted the data. HZ acquired the pathological data. FW contributed to the analysis and revision of the discussion section and prepared the pathological images. HW wrote the manuscript, and all authors analyzed the results and revised the manuscript. HZ made significant contributions to the conception and design of the study. HW, HZ, and FW confirm the authenticity of all the raw data. All authors have read and approved the final version of the manuscript.

Ethics approval and consent to participate

This study was approved by the Ethics Committee of Yantai Yuhuangding Hospital (Yantai, China; approval no. 2025-561).

Patient consent for publication

Written informed consent was obtained from the patient for the publication of any potentially identifiable images or data included in this article.

Competing interests

The authors declare that they have no competing interests.

Use of artificial intelligence tools

During the preparation of this work, AI tools were used to improve the readability and language of the manuscript or to generate images, and subsequently, the authors revised and edited the content produced by the AI tools as necessary, taking full responsibility for the ultimate content of the present manuscript.

References

1. Stacchiotti S, Baldi GG, Morosi C, Gronchi A and Maestro R: Extraskeletal myxoid chondrosarcoma: State of the art and current research on biology and clinical management. Cancers (Basel) 12: 2703, 2020.
2. Zhang L, Wang R, Xu R, Qin G and Yang L: Extraskeletal myxoid chondrosarcoma: A comparative study of imaging and pathology. Biomed Res Int 2018: 9684268, 2018.
3. Noguchi H, Mitsuhashi T, Seki K, Tochigi N, Tsuji M, Shimoda T and Hasegawa T: Fluorescence in situ hybridization analysis of extraskeletal myxoid chondrosarcomas using EWSR1 and NR4A3 probes. Hum Pathol 41: 336-342, 2010.
4. Wei S, Pei J, von Mehren M, Abraham JA, Patchefsky AS and Cooper HS: SMARCA2-NR4A3 is a novel fusion gene of extraskeletal myxoid chondrosarcoma identified by RNA next-generation sequencing. Genes Chromosomes Cancer 60: 709-712, 2021.

5. Zhu ZY, Wang YB, Li HY and Wu XM: Primary intracranial extraskeletal myxoid chondrosarcoma: A case report and review of literature. World J Clin Cases 10: 4301-4313, 2022.
6. Nodal S, Khalafallah AM, Sanghera BS, Garcia Barreto M, Errante EL, Levi AD, Ray WZ and Burks SS: A meta-analysis and systematic review: Association of timing and muscle strength after nerve transfer in upper trunk palsy. Neurosurg Rev 48: 503, 2025.
7. Mehta R and Chinthapalli K: Glasgow coma scale explained. BMJ 365: l1296, 2019.
8. Oken MM, Creech RH, Tormey DC, Horton J, Davis TE, McFadden ET and Carbone PP: Toxicity and response criteria of the eastern cooperative oncology group. Am J Clin Oncol 5: 649-655, 1982.
9. Kandoussi AE, Hung YP, Tung EL, Bauer F, Vicentini JRT, Lozano-Calderon S and Chang CY: Clinical, imaging and pathological features of extraskeletal myxoid chondrosarcoma. Skeletal Radiol 54: 959-966, 2025.
10. Okamoto S, Hisaoka M, Ishida T, Imamura T, Kanda H, Shimajiri S and Hashimoto H: Extraskeletal myxoid chondrosarcoma: A clinicopathologic, immunohistochemical, and molecular analysis of 18 cases. Hum Pathol 32: 1116-1124, 2001.
11. Giner F, López-Guerrero JA, Machado I, Rubio-Martínez LA, Espino M, Navarro S, Agra-Pujol C, Ferrández A and Llombart-Bosch A: Extraskeletal myxoid chondrosarcoma: p53 and Ki-67 offer prognostic value for clinical outcome-an immunohistochemical and molecular analysis of 31 cases. Virchows Arch 482: 407-417, 2023.
12. Ulucaköy C, Atalay İB, Yapar A, Kaptan AY, Bingöl İ, Doğan M and Ekşioğlu MF: Surgical outcomes of extraskeletal myxoid chondrosarcoma. Turk J Med Sci 52: 1183-1189, 2022.
13. Fice MP, Lee L, Kottamasu P, Almajnooni A, Cohn MR, Gusho CA, Gitelis S and Blank AT: Extraskeletal myxoid chondrosarcoma: A case series and review of the literature. Rare Tumors 14: 20363613221079754, 2022.
14. Chaskis C, Michotte A, Goossens A, Stadnik T, Koerts G and D'Haens J: Primary intracerebral myxoid chondrosarcoma. Case illustration. J Neurosurg 97: 228, 2002.
15. Scott RM, Dickersin R, Wolpert SM and Twitchell T: Myxochondrosarcoma of the fourth ventricle. Case report. J Neurosurg 44: 386-389, 1976.
16. Smith TW and Davidson RI: Primary meningeal myxochondrosarcoma presenting as a cerebellar mass: Case report. Neurosurgery 8: 577-581, 1981.
17. Salcman M, Scholtz H, Kristt D and Numaguchi Y: Extraskeletal myxoid chondrosarcoma of the falx. Neurosurgery 31: 344-348, 1992.
18. Sato K, Kubota T, Yoshida K and Murata H: Intracranial extraskeletal myxoid chondrosarcoma with special reference to lamellar inclusions in the rough endoplasmic reticulum. Acta Neuropathol 86: 525-528, 1993.
19. González-Lois C, Cuevas C, Abdullah O and Ricoy JR: Intracranial extraskeletal myxoid chondrosarcoma: Case report and review of the literature. Acta Neurochir (Wien) 144: 735-740, 2002.
20. Im SH, Kim DG, Park IA and Chi JG: Primary intracranial myxoid chondrosarcoma: Report of a case and review of the literature. J Korean Med Sci 18: 301-307, 2003.
21. Cummings TJ, Bridge JA and Fukushima T: Extraskeletal myxoid chondrosarcoma of the jugular foramen. Clin Neuropathol 23: 232-237, 2004.
22. Sorimachi T, Sasaki O, Nakazato S, Koike T and Shibuya H: Myxoid chondrosarcoma in the pineal region. J Neurosurg 109: 904-907, 2008.
23. O'Brien J, Thornton J, Cawley D, Farrell M, Keohane K, Kaar G, McEvoy L and O'Brien DF: Extraskeletal myxoid chondrosarcoma of the cerebellopontine angle presenting during pregnancy. Br J Neurosurg 22: 429-432, 2008.
24. Arpino L, Capuano C, Gravina M and Franco A: Parasellar myxoid chondrosarcoma: A rare variant of cranial chondrosarcoma. J Neurosurg Sci 55: 387-389, 2011.
25. Dulou R, Chargari C, Dagain A, Teriitehau C, Goasguen O, Jeanjean O and Védrine L: Primary intracranial extraskeletal myxoid chondrosarcoma. Neurol Neurochir Pol 46: 76-81, 2012.
26. Park JH, Kim MJ, Kim CJ and Kim JH: Intracranial extraskeletal myxoid chondrosarcoma: Case report and literature review. J Korean Neurosurg Soc 52: 246-249, 2012.
27. Qin Y, Zhang HB, Ke CS, Huang J, Wu B, Wan C, Yang CS and Yang KY: Primary extraskeletal myxoid chondrosarcoma in cerebellum: A case report with literature review. Medicine (Baltimore) 96: e8684, 2017.
28. Akakın A, Urgun K, Ekşi M, Yılmaz B, Yapıcıer Ö, Mestanoğlu M, Toktaş ZO, Demir MK and Kılıç T: Falcine myxoid chondrosarcoma: A rare aggressive case. Asian J Neurosurg 13: 68-71, 2018.
29. Kallen ME and Hornick JL: The 2020 WHO classification: What's new in soft tissue tumor pathology? Am J Surg Pathol 45: e1-e23, 2021.
30. Tekavec K, Švara T, Knific T, Gombač M and Cantile C: Histopathological and immunohistochemical evaluation of canine nerve sheath tumors and proposal for an updated classification. Vet Sci 9: 204, 2022.
31. Sarathy D, Snyder MH, Ampie L, Berry D and Syed HR: Dural convexity chondroma mimicking meningioma in a young female. Cureus 13: e20715, 2021.
32. Bellizzi AM: An algorithmic immunohistochemical approach to define tumor type and assign site of origin. Adv Anat Pathol 27: 114-163, 2020.
33. Almaghrabi A, Almaghrabi N and Al-Maghrabi H: Glomangioma of the kidney: A rare case of glomus tumor and review of the literature. Case Rep Pathol 2017: 7423642, 2017.
34. Velz J, Agaimy A, Frontzek K, Neidert MC, Bozinov O, Wagner U, Fritz C, Coras R, Hofer S, Bode-Lesniewska B and Rushing E: Molecular and clinicopathologic heterogeneity of intracranial tumors mimicking extraskeletal myxoid chondrosarcoma. J Neuropathol Exp Neurol 77: 727-735, 2018.
35. Liu Z, Bian J, Yang Y, Wei D and Qi S: Ewing sarcoma of the pancreas: A pediatric case report and narrative literature review. Front Oncol 14: 1368564, 2024.
36. Dulken BW, Kingsley L, Zdravkovic S, Cespedes O, Qian X, Suster DI and Charville GW: CHRNA6 RNA in situ hybridization is a useful tool for the diagnosis of extraskeletal myxoid chondrosarcoma. Mod Pathol 37: 100464, 2024.
37. Ngo C, Verret B, Vibert J, Cotteret S, Levy A, Pechoux CL, Haddag-Miliani L, Honore C, Faron M, Quinquis F, *et al*: A novel fusion variant LSM14A::NR4A3 in extraskeletal myxoid chondrosarcoma. Genes Chromosomes Cancer 62: 52-56, 2023.
38. Wilbur HC, Robinson DR, Wu YM, Kumar-Sinha C, Chinnaiyan AM and Chugh R: Identification of novel PGR-NR4A3 fusion in extraskeletal myxoid chondrosarcoma and resultant patient benefit from tamoxifen therapy. JCO Precis Oncol 6: e2200039, 2022.
39. Hong YG, Yoo J, Kim SH and Chang JH: Intracranial extraskeletal myxoid chondrosarcoma in fourth ventricle. Brain Tumor Res Treat 9: 75-80, 2021.